

# Radio structures of the nuclei of nearby Seyfert galaxies and the nature of the missing diffuse emission

M. Orienti<sup>1,2\*</sup>, M.A. Prieto<sup>1</sup>

<sup>1</sup>*Instituto de Astrofísica de Canarias, c/ Vía Láctea s/n, E-38205 La Laguna (Tenerife), Spain*

<sup>2</sup>*Istituto di Radioastronomia - INAF, Via P. Gobetti 101, I-40129 Bologna, Italy*

Received 29 October 2018; accepted ?

## ABSTRACT

We present archival high spatial resolution VLA and VLBA data of the nuclei of seven of the nearest and brightest Seyfert galaxies in the Southern Hemisphere. At VLA resolution ( $\sim 0.1$  arcsec), the nucleus of the Seyfert galaxies is unresolved, with the exception of MCG-5-23-16 and NGC 7469 showing a core-jet structure. Three Seyfert nuclei are surrounded by diffuse radio emission related to star-forming regions. VLBA observations with parsec-scale resolution pointed out that in MRK 1239 the nucleus is clearly resolved in two components separated by  $\sim 30$  pc, while the nucleus of NGC 3783 is unresolved. Further comparison between VLA and VLBA data of these two sources shows that the flux density at parsec scales is only 20% of that measured by the VLA. This suggests that the radio emission is not concentrated in a single central component, as in elliptical radio galaxies, and an additional low-surface brightness component must be present. A comparison between Seyfert nuclei with different radio spectra points out that the “presence” of undetected flux on milli-arcsecond scale is common in steep-spectrum objects, while in flat-spectrum objects essentially all the radio emission is recovered. In the steep-spectrum objects, the nature of this “missing” flux is likely due to non-thermal AGN-related radiation, perhaps from a jet that gets disrupted in Seyfert galaxies because of the denser environment of their spiral hosts.

**Key words:** galaxies: active - galaxies: Seyfert - radio continuum: general

## 1 INTRODUCTION

Only a small fraction ( $\sim 10\%$ ) of the population of active galactic nuclei (AGN) possess a powerful radio emission ( $L_{1.4\text{ GHz}} > 10^{23}$  W/Hz), as found in radio galaxies/quasars and blazars. Seyfert galaxies are part of the “radio-quiet” AGN population, with radio luminosity  $L_{1.4\text{ GHz}} \leq 10^{20-23}$  W/Hz. Despite their weak radio emission, Seyfert nuclei are very nearby, allowing the study in detail of the radio properties of their central engine.

Radio observations with arcsecond resolution of several Seyfert samples (see e.g. Ulvestad & Wilson 1984; Morganti et al. 1999; Thean et al. 2000) showed that a large fraction of Seyferts have resolved structures, with hint of jets and/or extended emission, the latter usually related to star-forming regions. Several objects, such as NGC 1052 (Wrobel 1984), NGC 1068 (Ulvestad et al. 1987), NGC 7674 (Momjian et al. 2003), and MRK 3 (Kukula et al. 1999) have been found to display a radio morphology with core, collimated jets and hot spots, similar to those found in radio-loud galaxies. However, powerful radio sources have linear

structures reaching hundreds of kpc or even Mpc scales, while in Seyferts the radio emission is confined to a few kpc or even sub-kpc scales.

When observed with milli-arcsecond resolution, the pc-scale structure of Seyfert nuclei is usually resolved in several components (e.g. NGC 3079, Trotter et al. 1998), resembling a jet structure (e.g. NGC 4151, Ulvestad et al. 1998; Nagar et al. 2001) and sometimes with the presence of extended emission (e.g. NGC 5793, Hagiwara et al. 2000). The comparison between arcsec and milli-arcsec radio properties pinpointed a frequent misalignment between pc and kpc-scale jets, suggesting either a change in jet ejection axis, or a bending due to pressure gradients in the ambient medium (Middelberg et al. 2004).

An intriguing characteristic shown by a large number of Seyfert nuclei is that the radio emission arising from their pc-scale structure is often much fainter than that derived from observations with lower resolution, even in the case the nucleus is unresolved. This result suggests that in Seyfert nuclei the radio emission is not concentrated in the central region, as found in powerful radio galaxies, but it extends on scales of tens or hundreds pc (see e.g. Sadler et al. 1995). However, not all the Seyfert nuclei have missing flux

\* E-mail: orienti@ira.inaf.it

on parsec scales, as in the case of MRK 530 (Lal et al. 2004), indicating that the radio emission mainly arises from the central compact component, without evidence of extended, low-surface brightness features.

In this paper, we present the results of multi-frequency archival VLA and/or VLBA data of a sample of some of the nearest and brightest Seyfert galaxies, taken from the infrared high spatial resolution studies conducted by Prieto et al. (2009) and Reunanen et al. (2009). For these sources, no complete and/or unambiguous information on their radio properties could be found in the literature. The comparison between these data with those at pc-scale resolution available from the literature allows a better determination of the physical conditions of the radio emission at kpc and pc scales.

Throughout this paper, we assume the following cosmology:  $H_0 = 71 \text{ km s}^{-1} \text{ Mpc}^{-1}$ ,  $\Omega_M = 0.27$ , and  $\Omega_\Lambda = 0.73$ , in a flat Universe. The spectral index is defined as  $S(\nu) \propto \nu^{-\alpha}$ .

## 2 THE SAMPLE

The objects studied in this paper are part of the sample of Seyfert nuclei from Prieto et al. (2009) and Reunanen et al. (2009). They consist in the nearest and brightest Seyfert nuclei accessible from the Southern Hemisphere. The proximity of these objects allows us to study them at scales of a few tens of parsec in the IR with VLT - adaptive optics and interferometry which deliver spatial resolutions comparable to that achieved in the optical with HST, and in radio with VLA and VLBI. In Fig. 1 we present VLT-VISIR images at  $11.8 \mu\text{m}$  of the Seyfert studied in this paper. Details on VISIR observations and data reduction can be found in Reunanen et al. (2009). The dominant IR emission comes from the central nucleus that is unresolved with FWHM  $< 0.35$  arcsec, which corresponds to linear sizes between 30 and 190 pc, depending on the redshift. In NGC 7469 and NGC 7582, an additional emission from the star forming regions is clearly detected.

High spatial resolution spectral energy distribution (SED) have been produced for these objects. For the majority of the Seyfert considered, multi-frequency, high-resolution information in the radio band has not been exploited in full. For this reason, we collected and analysed archival radio data with (sub-)arcsecond resolution in order to implement the information already available and to constrain the radio emission from these nuclei.

The list of the Seyfert nuclei studied in this paper is in Table 1. We considered only datasets at frequencies and resolution not available in the literature, or for which no unambiguous information could be found.

### 2.1 Radio properties of the selected sources

#### 2.1.1 NGC 1097

NGC 1097 is a barred spiral galaxy hosting a Seyfert 1 nucleus (Storchi-Bergmann et al. 1993). The radio emission is dominated by a ring-like structure related to star-forming regions also detected in optical. At the centre of the ring

there is an unresolved (beam  $\sim 0.3$  arcsec at 8.4 GHz) component (Thean et al. 2000) with an inverted non-thermal spectrum (Morganti et al. 1999). The radio core was observed by Sadler et al. (1995) with the Parkes-Tidbinbilla interferometer (PTI) that provides a resolution  $< 0.1$  arcsec. No radio emission was detected, implying that the core flux density is  $< 5$  mJy at 2.3 GHz.

#### 2.1.2 MCG-5-23-16

MCG-5-23-16 is a S0 galaxy hosting a Seyfert 2 nucleus. Its radio properties were studied by Ulvestad & Wilson (1984) with VLA observations at 1.4 and 4.8 GHz. The radio structure of the nucleus is found slightly resolved (beam  $\sim 0.4$  arcsec at 4.8 GHz) with a spectral index  $\alpha \sim 0.5$ . No evidence of extra-nuclear emission was detected.

High spatial resolution (beam  $< 0.1$  arcsec) observations with PTI (Sadler et al. 1995) could set only an upper limit to the flux density of the core  $S_{8.4\text{GHz}} < 7$  mJy.

#### 2.1.3 MRK 1239

MRK 1239 is an early-type E/S0 galaxy hosting a Seyfert 1.5 nucleus. Its central radio structure was studied by Ulvestad et al. (1995) and Rush et al. (1996) with the VLA. The source appears unresolved at all frequencies (beam  $\sim 0.2$  arcsec at 8.4 GHz) without evidence of extended emission surrounding the nucleus. Ulvestad et al. (1995) noted a strong steepness in the radio spectrum between 4.8 and 8.4 GHz ( $\alpha \sim 1.6$ ), that they interpreted as due to flux variability (observations were not carried out simultaneously).

#### 2.1.4 NGC 3783

NGC 3783 is a barred spiral galaxy with a highly variable Seyfert 1 nucleus. Multi-frequency radio VLA observations by Ulvestad & Wilson (1984), Unger et al. (1986) and Schmitt et al. (2001) pointed out the presence of an unresolved component (beam  $\sim 0.25$  arcsec at 8.4 GHz) with a spectral index  $\alpha \sim 0.5$ . No extended extra-nuclear emission was found. High spatial resolution (beam  $< 0.1$  arcsec) observations with PTI (Sadler et al. 1995) could set only an upper limit to the flux density of the core  $S_{1.6\text{GHz}} < 6$  mJy.

#### 2.1.5 NGC 5506

NGC 5506 is a spiral galaxy with a Seyfert 2 nucleus. The central radio structure was studied by Ulvestad et al. (1981) and Unger et al. (1986) by VLA and MERLIN observations. It shows a diffuse bubble-like feature extending to the north-west of the unresolved nucleus. At 5 GHz Wehrle & Morris (1987) found a low-surface brightness halo enshrouding the central structures.

Multi-frequency observations of the nucleus with the PTI (Sadler et al. 1995) showed that it has a convex spectrum. Pc-scale VLBI observations at 18, 6 and 3.6 cm

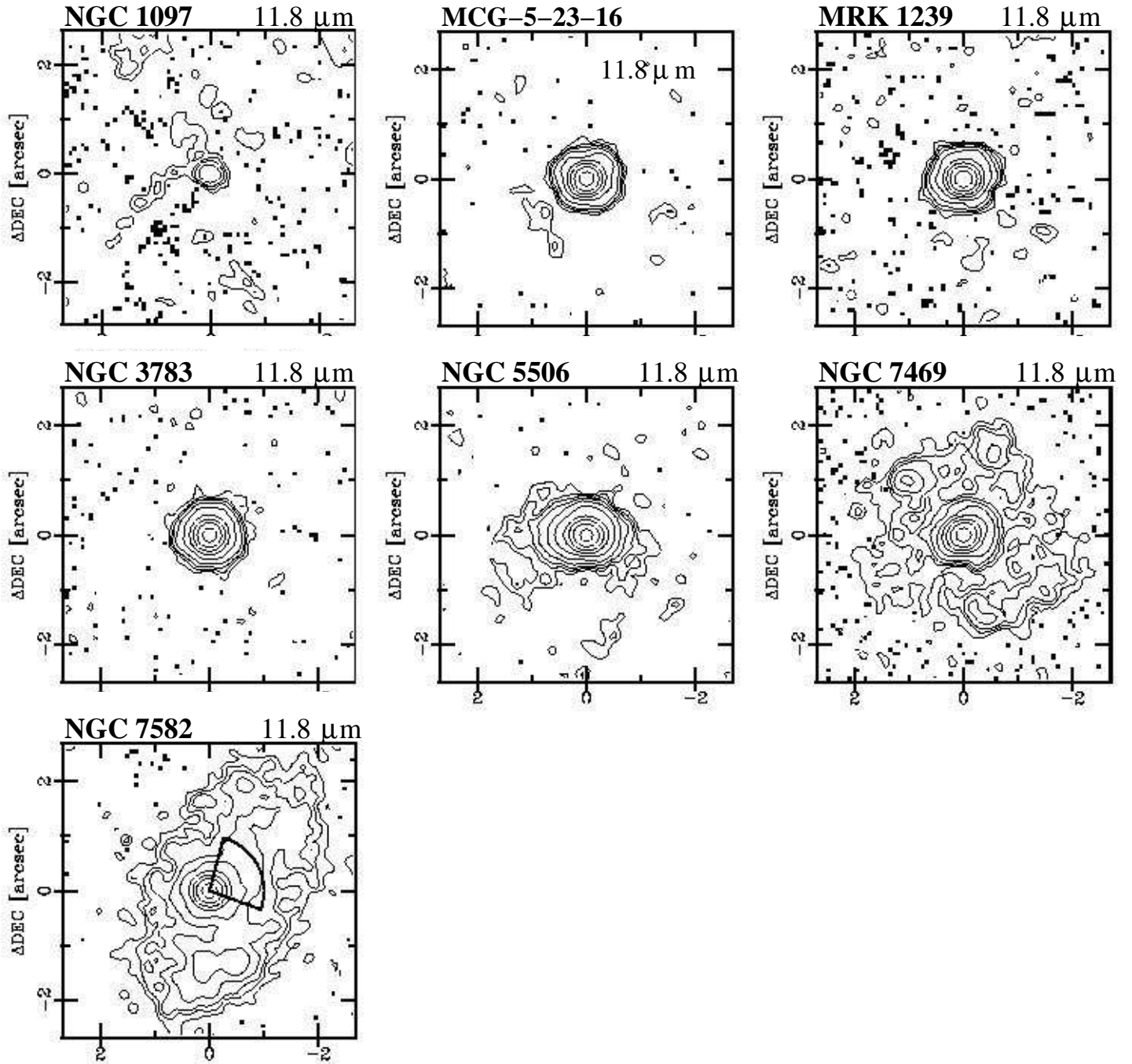


**Figure 1.** VLT-VISIR images at  $11.8 \mu\text{m}$  of the Seyfert nuclei studied in this paper. Images adapted from Reunanen et al. (2009). Contours are at  $3\sigma$ , 5, 7, 11 and 19 levels. The triangle in NGC 7582 represents the ionization cone.

(Middelberg et al. 2004) could resolve the nucleus in three main components roughly aligned in the east-west direction and extending within an area of about 50 mas ( $\sim 6$  pc). The flattish spectrum displayed by the brightest component suggests that it is the true source core.

### 2.1.6 NGC 7469

NGC 7469 is a spiral galaxy with a Seyfert 1 nucleus embedded in a ring of starburst activity. At radio frequencies, its structure shows an unresolved central component surrounded by a ring of star-forming regions (Wilson et al. 1991). MERLIN observations with high spatial resolution (beam  $\sim 0.05$  arcsec) showed that the nucleus is clearly resolved in two components with a core-jet structure elongated in the east-west direction. VLBI observations (beam

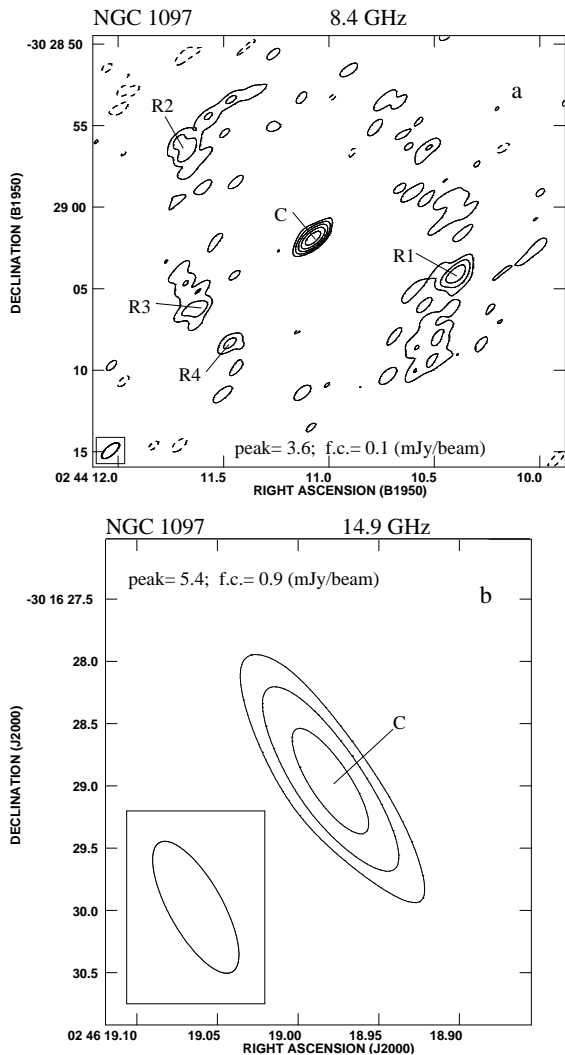


**Figure 2.** VLA images at 8.4 GHz (*top*) and at 14.9 GHz (*bottom*) of the central region of NGC 1097. On each image we provide the observing frequency; the restoring beam, plotted on the bottom left corner; the peak flux density in mJy/beam; the first contour intensity (*f.c.* in mJy/beam), that is 3 times the off-source noise level; contour levels increase of a factor 2.

$\sim 10$  mas) at 1.6 GHz (Lonsdale et al. 2003) could resolve the core-jet structure in five different components, lying in an east-west line as found in the lower resolution MERLIN image, and contained in an area of about 168 mas ( $\sim 55$  pc).

### 2.1.7 NGC 7582

NGC 7582 is a barred spiral galaxy hosting a Seyfert 2 nucleus surrounded by a star forming ring. Its radio structure shows an unresolved central component embedded in a diffuse emission related to the star-forming region also detected in the optical (Ulvestad & Wilson 1984). The extended emission is elongated in the NW-SE direction, with a spectral index  $\alpha \sim 0.7$  (Morganti et al. 1999). High

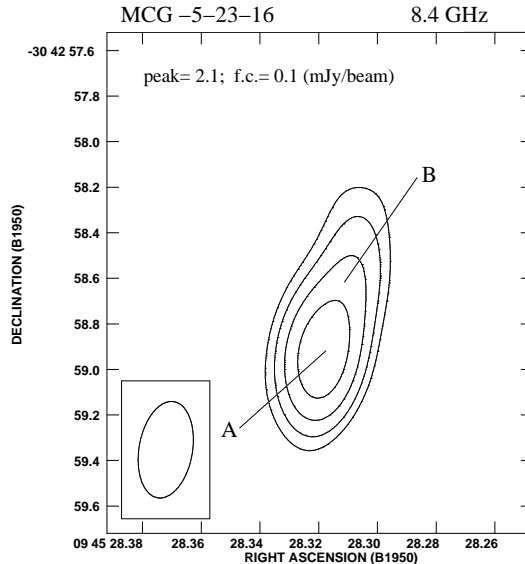


**Figure 3.** VLA image at 8.4 GHz of the central region of MCG-5-23-16. On the image we provide the observing frequency; the restoring beam, plotted on the bottom left corner; the peak flux density in mJy/beam; the first contour intensity (*f.c.* in mJy/beam), that is 3 times the off-source noise level; contour levels increase of a factor 2.

**Table 1.** The Seyfert sample. Column 1: source name; col. 2: type; col. 3: redshift; col. 4: luminosity distance; col. 5: scale.

Source	Type	$z$	$D_L$	kpc/''
NGC 1097	1	0.00424	18.0	0.086
MCG-5-23-16	2	0.008486	36.1	0.172
MRK 1239	1.5	0.02883	124.5	0.570
NGC 3783	1	0.009730	41.4	0.197
NGC 5506	2	0.006181	26.2	0.126
NGC 7469	1	0.016317	69.8	0.328
NGC 7582	2	0.005254	22.3	0.107

spatial resolution (beam  $< 0.1$  arcsec) observations with PTI (Sadler et al. 1995) could set only an upper limit to the flux density of the core  $S_{8.4\text{GHz}} < 5$  mJy.

## 3 NEW RADIO DATA

Archival VLA/VLBA radio data of the aforementioned sample were analysed in order to implement the information available in the literature. To achieve an adequate spatial resolution to resolve the nuclear structure, we considered observations carried out when the VLA was in one of the extended configuration (array A or B) at frequencies ranging between 1.4 and 14.9 GHz, when available. We reduced datasets either at frequencies lacking information

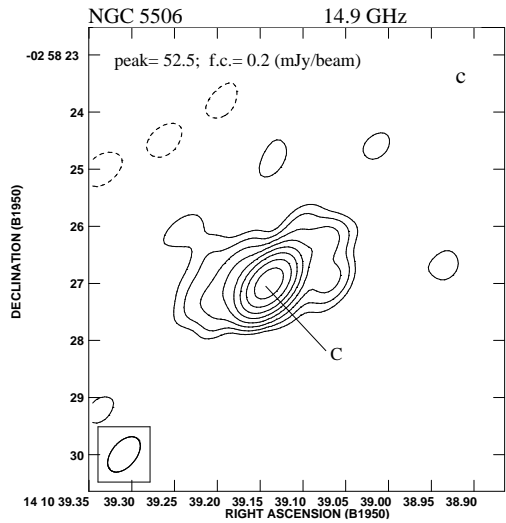
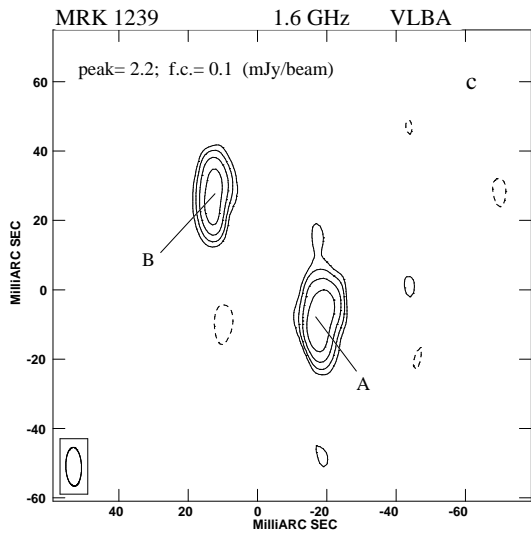
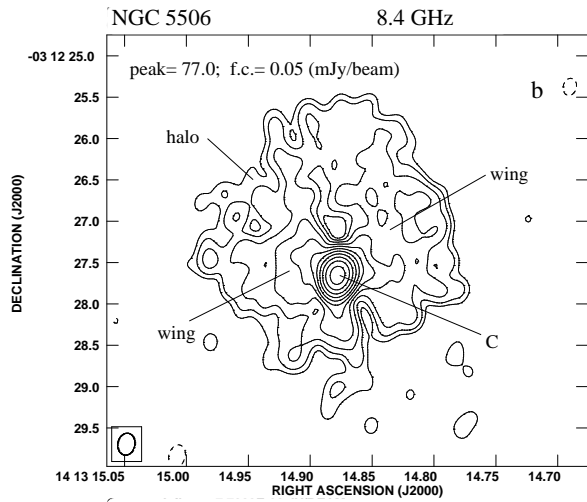
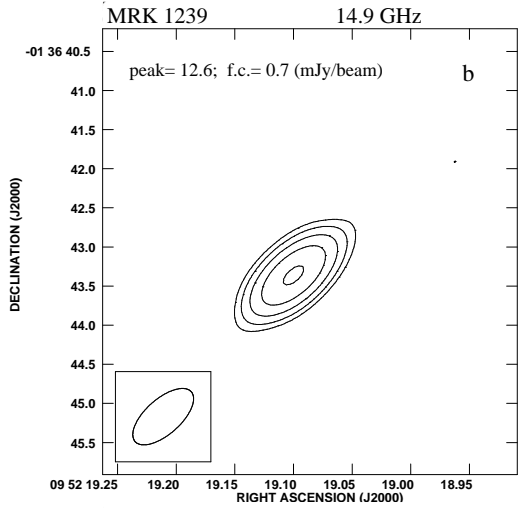
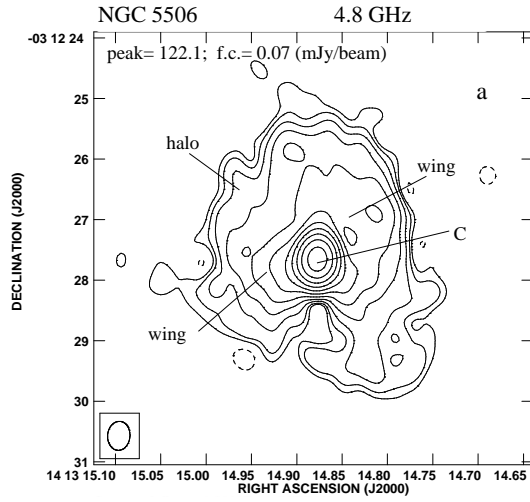
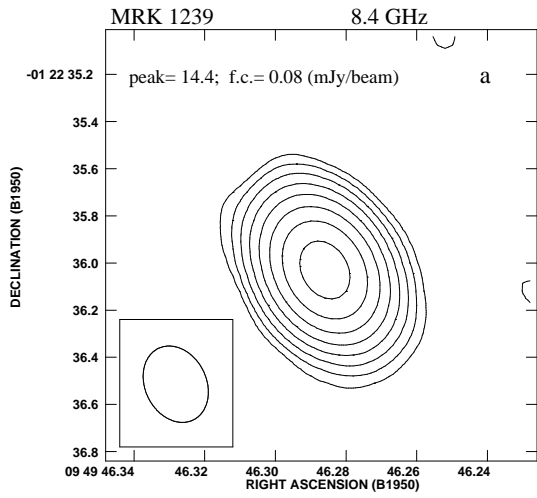


**Figure 4.** VLA images at 8.4 GHz (*top*), and 14.9 GHz (*centre*), and VLBA image at 1.6 GHz (*bottom*) of the central region of MRK 1239. On each image we provide the observing frequency; the restoring beam, plotted on the bottom left corner; the peak flux density in mJy/beam; the first contour intensity (*f.c.* in mJy/beam), that is 3 times the off-source noise level; contour levels increase of a factor 2.

**Figure 5.** VLA images at 4.8 GHz (*top*), 8.4 GHz (*centre*), and 14.9 GHz (*bottom*) of the central region of NGC 5506. On each image we provide the observing frequency; the restoring beam, plotted on the bottom left corner; the peak flux density in mJy/beam; the first contour intensity (*f.c.* in mJy/beam), that is 3 times the off-source noise level; contour levels increase of a factor 2.

or for which data presented in the literature were not found satisfactory.

The data reduction was carried out following the standard procedures for the VLA implemented in the NRAO AIPS package. Images were produced after a few phase-only calibration iterations. In order to obtain accurate flux density at 1.4 GHz, it was necessary to image several confusing sources falling within the primary beam. Uncertainties in the determination of flux density are dominated by amplitude calibration errors, which are between 3% and 5%, being worse at 14.9 GHz. The rms noise level ( $1\sigma$ ) on the image plane is usually below 0.1 mJy, being irrelevant for our targets, with the exceptions of NGC 1097 and MCG-5-23-16 where it is comparable to the amplitude calibration errors.

In the case of NGC 1097, MRK 1239 and NGC 3783, for which no information on their pc-scale structure could be found in the literature, we reduced archival VLBA data. No archival VLBA data were found for the sources MCG-5-23-16 and NGC 7582. The Seyfert nuclei considered in this paper are not bright enough to give detectable fringes. VLBI fringe fitting was done on a bright source lying close to the target, and off-beam phase referencing was performed to calibrate the phases of the target source. In the case of NGC 1097, no signal of the source was detected. For MRK 1239 and NGC 3783, the structure was visible from the first image with a  $4\sigma$  noise level. Then phase self-calibration with a solution interval of 30s was performed using the CLEAN component model. After a few iterations we use natural weights to pick up possible extended emission. No amplitude calibration was performed due to the weakness of the targets.

## 4 RESULTS

### 4.1 Radio images

Full resolution VLA images of the sources discussed in this paper are presented in Figs. 2 to 7. In the case of NGC 7469 and NGC 7582, where an extended diffuse emission is present around the central nucleus, an image without the shortest baselines was produced in order to better describe the compact components without the contamination from the low-surface brightness extended emission (Figs. 6b and 7b). For MRK 1239 and NGC 3783, VLBA images at 1.6 GHz are presented in Figs. 4c and 8 respectively.

Flux density and angular size were measured by means of the task JMFIT, which performs a Gaussian fit on the image plane. In case of extended structures, the flux density was derived by TVSTAT, while the source size was measured from the lowest contour on the image plane. The nucleus of these Seyfert galaxies is unresolved or marginally resolved in VLA observations. We consider marginally resolved those nuclei whose largest angular size (LAS) is between 0.5 and 1 beam size at the best resolution, and we term unresolved those whose LAS is smaller than half of the beam.

Source parameters, together with information on the observations, are reported in Table 2. In Table 3, we present the observational parameters of the source components.

**Table 3.** Radio properties of the source components. Col. 1: source name; col. 2: source component, the name refers to the label as reported in Figs. from 2 to 8; col. 3: observing frequency; col. 4: flux density; cols. 5 and 6: deconvolved major and minor axis. *a*: values derived on VLBA images.

Source	Comp.	Freq. GHz	Flux mJy	$\theta_{\max}$ arcsec	$\theta_{\min}$ arcsec
(1)	(2)	(3)	(4)	(5)	(6)
NGC 1097	C	8.4	4.0	<0.5	-
	C	14.9	5.6	<0.5	-
	R1	8.4	1.8	0.9	0.7
	R2	8.4	0.8	1.7	1.3
MCG-5-23-16	R3	8.4	0.6	1.6	0.8
	A	8.4	2.1	<0.1	-
	B	8.4	0.5	<0.1	-
	C	1.4	60.0	<0.3	-
MRK 1239	C	5.0	26.8	<0.1	-
	C	8.4	15.5	<0.1	-
	C	14.9	9.3	<0.2	-
	A <sup>a</sup>	1.6	6.0	0.013	0.006
NGC 3783	B <sup>a</sup>	1.6	4.2	0.013	0.004
	C <sup>a</sup>	1.6	4.6	0.022	0.007
NGC 5506	C	1.4	304.0	<1.0	-
	C	4.8	136.0	<0.1	-
	C	8.4	84.0	<0.08	-
	C	14.9	58.0	<0.2	-
	Wing	4.8	27	2.4	2.0
	Wing	8.4	16	2.2	1.7
NGC 7469	Halo	4.8	18	4.2	3.0
	Halo	8.4	11	3.8	3.2
	C	8.4	14.8	<0.14	-
	C	14.9	10.6	0.1	<0.05
NGC 7582	R1	8.4	0.3	0.8	0.4
	R2	8.4	0.6	0.9	0.7
	R3	8.4	0.7	1.1	0.8
	C	4.9	9.5	0.8	<0.1
	C	8.4	6.9	0.4	0.2
	R1	4.9	3.6	0.4	0.3
NGC 7469	R1	8.4	2.1	0.3	0.3
	R2	4.9	0.8	0.3	<0.1
	R3	4.9	1.1	0.5	0.3

### 4.2 Notes on individual sources

In this section we describe the characteristics of the Seyfert nuclei arising from the new images presented in this paper.

#### 4.2.1 NGC 1097

The new images at 8.4 and 14.9 GHz are presented in Fig. 2, and have a resolution of  $0''.66 \times 0''.25$  and  $1''.15 \times 0''.45$  respectively. Fig. 2a shows for the first time the ring structure at 8.4 GHz. Four star-forming regions, labelled R1, R2, R3 and R4 in Fig. 2a, are also present at 1.4 and 5 GHz (see e.g. Hummel et al. 1987). The central component appears unresolved in both 8.4 and 14.9 GHz images, giving an upper limit to its linear size of  $< 0''.5$  ( $< 43$  pc). The spectral index is found inverted between 1.4 and 14.9 GHz.

**Table 2.** Radio observations and source parameters for the Seyfert galaxies. Column 1: source name; col. 2: observing frequency; col. 3: array configuration; col. 4: beam size; col. 5: observing date; col. 6: flux density; col. 7: luminosity; col. 8: largest angular size; col. 9: largest linear size; col. 10: morphology of the nuclear component (Un=unresolved, MR= marginally resolved; Double=two well-separated components); col. 11: morphology of the extended structure, when present.

Source	Freq. GHz	conf	beam arcsec	Obs. date	Flux density mJy	Log P W/Hz	LAS arcsec	LLS pc	Morph.	Ext
(1)	(2)	(3)	(4)	(5)	(6)	(7)	(8)	(9)	(10)	(11)
NGC 1097	8.4	A	0.66×0.25	Oct 31 1992	30.0	21.04	18	1550	Un	Ring
NGC 1097	14.9	B	1.15×0.45	Feb 24 2001	5.0	20.30	<0.5	< 48	Un	No
MCG-5-23-16	8.4	A	0.43×0.23	Aug 21 1999	2.6	20.60	1.2	206	MR	No
MRK 1239	1.4	A	1.54×1.25	Jan 16 1993	60.0	23.04	<0.3	<171	Un	No
MRK 1239	4.8	A	0.46×0.40	Jul 31 1987	27.0	22.60	<0.1	<57	Un	No
MRK 1239	8.4	A	0.33×0.26	Jan 16 1993	15.0	22.44	<0.1	<57	Un	No
MRK 1239	8.4	A	0.26×0.22	Jul 15 1995	14.5	22.44	<0.1	<57	Un	No
MRK 1239	14.9	B	0.97×0.42	Dec 15 2003	9.0	22.22	<0.2	114	Un	No
MRK 1239	1.6	VLBA	0.011×0.004	May 09 2005	10.2	22.26	0.070	40	Double	No
NGC 3783	1.6	VLBA	0.028×0.008	Nov 30 1999	4.6	20.95	0.022	4.3	Un	No
NGC 5506	1.4	A	1.71×1.24	May 06 2002	324.0	22.42	4.0	500	Un	Halo
NGC 5506	4.8	A	0.48×0.37	May 06 2002	181.6	22.11	4.2	530	Un	Halo
NGC 5506	8.4	A	0.27×0.20	Nov 14 2000	111.6	21.96	3.8	480	Un	Halo
NGC 5506	14.9	B	0.72×0.43	Dec 05 1991	65.0	21.72	3.3	415	Un	Halo
NGC 7469	8.4	A	0.22×0.19	Feb 05 2006	31.4	22.26	3.1	1200	MR	Ring
NGC 7469	14.9	A	0.14×0.10	Sep 08 1999	10.6	21.71	0.1	33	MR	No
NGC 7582	4.8	A	1.25×0.32	Dec 12 2000	75.0	21.64	10	1070	Un	Ring
NGC 7582	8.4	A	0.75×0.19	Dec 12 2000	42.0	21.34	6	640	Un	Ring

#### 4.2.2 MCG-5-23-16

The VLA image at 8.4 GHz (Fig. 3), with a resolution of  $0''.43 \times 0''.23$ , is presented for the first time. The source is resolved in the north direction, suggesting the presence of a jet-like structure. The total radio spectrum shows a slight steepening at 8.4 GHz with a spectral index  $\alpha = 0.8 \pm 0.1$ .

#### 4.2.3 MRK 1239

New 14.9-GHz VLA and 1.6-GHz VLBA images are presented in Figs. 4b,c with resolution of  $0''.97 \times 0''.42$  and  $0''.011 \times 0''.004$  respectively. The central structure is unresolved in our VLA images at all frequencies, giving an upper limit to the linear size of  $< 57$  pc (Figs. 4a,b). The spectral index we obtain is  $\alpha \sim 0.9 \pm 0.1$  without any evidence of the steepening reported by Ulvestad et al. (1995) (see Section 2.1.3), and in a better agreement with what found by Rush et al. (1996). It is worth noting that data reported by Rush et al. (1996) refer to low resolution observations carried out when the VLA was in D-configuration. The good agreement between these values and our measurements suggests that no extended emission on kpc scales is present. When observed with pc-scale resolution, the nucleus of MRK 1239 at 1.6 GHz is resolved in two components separated by  $\sim 50$  mas ( $\sim 30$  pc), with position angle of  $40^\circ$  (Fig. 4c). The lack of multi-frequency observations with similar resolution does not allow us to study the spectral index of these components.

The flux density measured on the VLBA image at 1.6 GHz is 10.2 mJy, i.e. only 20% of the VLA flux density at 1.6 GHz, obtained re-scaling the 1.4 GHz VLA flux density

with the spectral index computed between 1.4 and 4.8 GHz ( $\alpha = 0.6$ ). This indicates that almost 80% of the flux density measured with the VLA is missing in the VLBA image.

#### 4.2.4 NGC 3783

The VLBA image at 1.6 GHz, with a resolution of  $0''.028 \times 0''.008$  (Fig. 8), is presented for the first time. In this image, the nucleus is unresolved with a linear size  $< 4$  pc. The total flux density measured on the VLBA image is 4.6 mJy, that represents only a 20% of the flux density of the unresolved component in VLA observations (Unger et al. 1986). This indicates that the majority ( $\sim 80\%$ ) of the flux measured with the VLA is missing in the VLBA image.

#### 4.2.5 NGC 5506

New VLA images at 4.8 and 8.4 GHz with resolution of  $0''.48 \times 0''.37$  and  $0''.27 \times 0''.20$  respectively, are shown in Fig. 5a,b. The source displays an unresolved central component with a diffuse wing-like emission extending mainly to the north-west and east part of the nucleus. The high dynamic range, namely the ratio between the peak flux density and  $1\sigma$  noise level, of our images allows us to detect also at 8.4 GHz the extended low-surface brightness halo (Figs. 5a,b). This has a diameter of  $\sim 2''.75$  ( $\sim 350$  pc) enshrouding the central features. The nucleus is unresolved in our VLA images, giving an upper limit of  $< 0''.08$  ( $< 10$  pc). The nucleus accounts for the

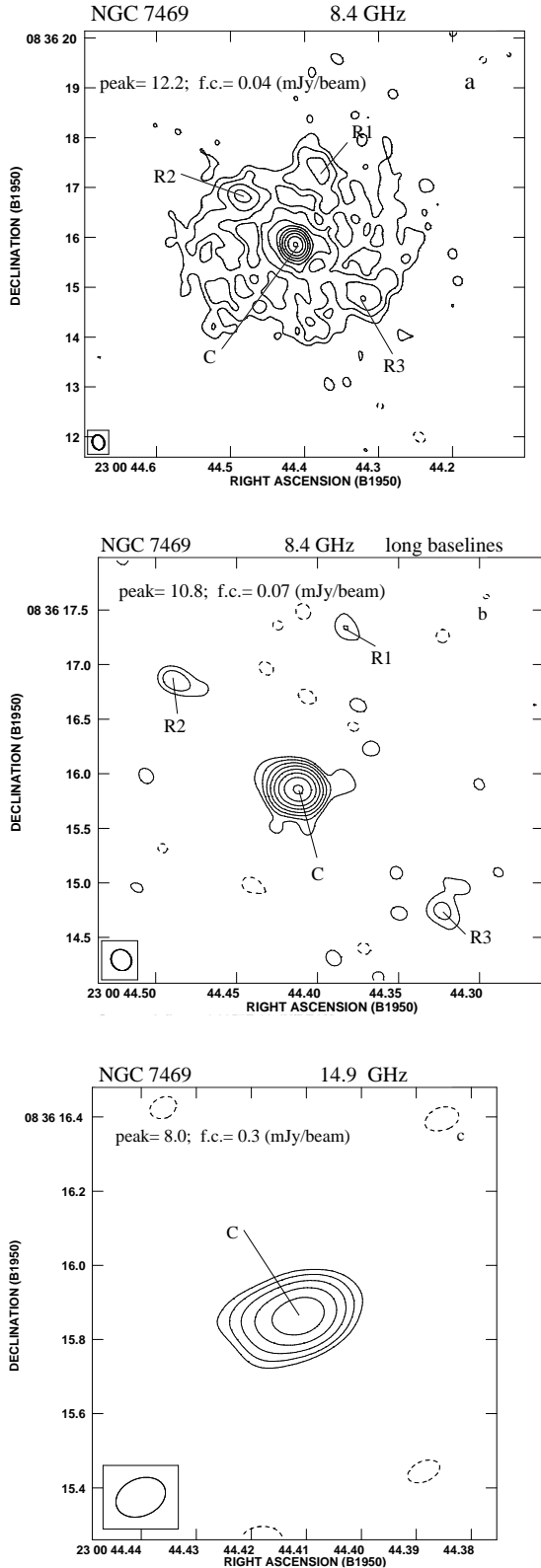


**Figure 6.** VLA images of the central region of NGC 7469 at 8.4 GHz (*top*), without the shortest baselines (*centre*), and at 14.9 GHz (*bottom*). On each image we provide the observing frequency; the restoring beam, plotted on the bottom left corner; the peak flux density in mJy/beam; the first contour intensity (*f.c.* in mJy/beam), that is 3 times the off-source noise level; contour levels increase of a factor 2.

majority (75%) of the radio emission. Its spectral index is  $\alpha \sim 0.8 \pm 0.1$ . The low-surface brightness halo and the extended wing-like structures have a slightly steeper spectral index  $\alpha = 0.9 \pm 0.1$ .

A comparison between simultaneous MERLIN and EVN observations at 18 and 6 cm clearly indicates that almost 43% of the flux density detected by MERLIN cannot be recovered in EVN images (Middelberg et al. 2004). In fact, a diffuse emission, detected by MERLIN observations, is not seen by the EVN, as the EVN is insensitive to structures larger than 35 and 11 mas at 18 and 6 cm, respectively.

#### 4.2.6 NGC 7469

We produced new VLA image at 8.4 GHz with a resolution of  $0''.2 \times 0''.18$  (Fig. 6b) obtained without the shortest ( $< 35$  k $\lambda$ ) baselines in order to pinpoint the compact central structure and to reduce the contamination from the surrounding ring. The radio emission is dominated by an unresolved central component surrounded by a ring of star-forming regions with a diameter of about  $3''.7$  ( $\sim 1.2$  kpc). In our new image at 14.9 GHz (Fig. 6c), the nucleus is elongated in the east-west direction. The spectral index is  $\alpha \sim 0.5 \pm 0.1$ . The elongation is in agreement with that shown by MERLIN (Alberdi et al. 2006) and VLBI (Lonsdale et al. 2003) images where the nucleus clearly shows a core-jet structure elongated in the same direction. In the diffuse extranuclear emission, three clumps of star-forming regions, labelled R1, R2, and R3 in Figs. 6a,b, are clearly visible at 8.4 GHz.

A comparison between MERLIN and VLBA images clearly indicates that almost 50% of the flux density detected by MERLIN (FWHM  $\sim 0''.15$ , Thean et al. 2001) is missing in the VLBA image at the same frequency (Lonsdale et al. 2003).

#### 4.2.7 NGC 7582

We produced new VLA image at 4.8 GHz with a resolution of  $0''.94 \times 0''.24$  (Fig. 7b) obtained without the shortest ( $< 45$  k $\lambda$ ) baselines in order to pinpoint the compact central structure and to reduce the contamination from the surrounding extended emission. The radio emission is dominated by an unresolved central component surrounded by diffuse emission related to star-forming regions (Fig. 7), also detected in the optical. The nucleus, with a spectral index  $\alpha \sim 0.6 \pm 0.1$ , is unresolved at all frequencies, giving an upper limit of about  $0''.4$  ( $< 40$  pc) to its linear size. The extended emission has a maximum diameter of about  $9''$  ( $\sim 950$  pc) and a spectral index  $\alpha \sim 1.0 \pm 0.1$ , that is steeper than the value ( $\alpha \sim 0.7$ ) found by Morganti et al. (1999). The discrepancy may arise from the different resolution of the observations taken into account. Three compact regions, labelled R1, R2, R3 in Figs. 7a and 7b, are present in the diffuse emission at 4.8 GHz. For these clumps, near-infrared counterpart was found by Fernandez-Ontiveros (2009, in preparation) suggesting that they are star-forming regions. Component R1 is visible also at 8.4 GHz, with a flux density of  $\sim 2.1$  mJy, and a spectral index  $\alpha \sim 0.9 \pm 0.2$ ,



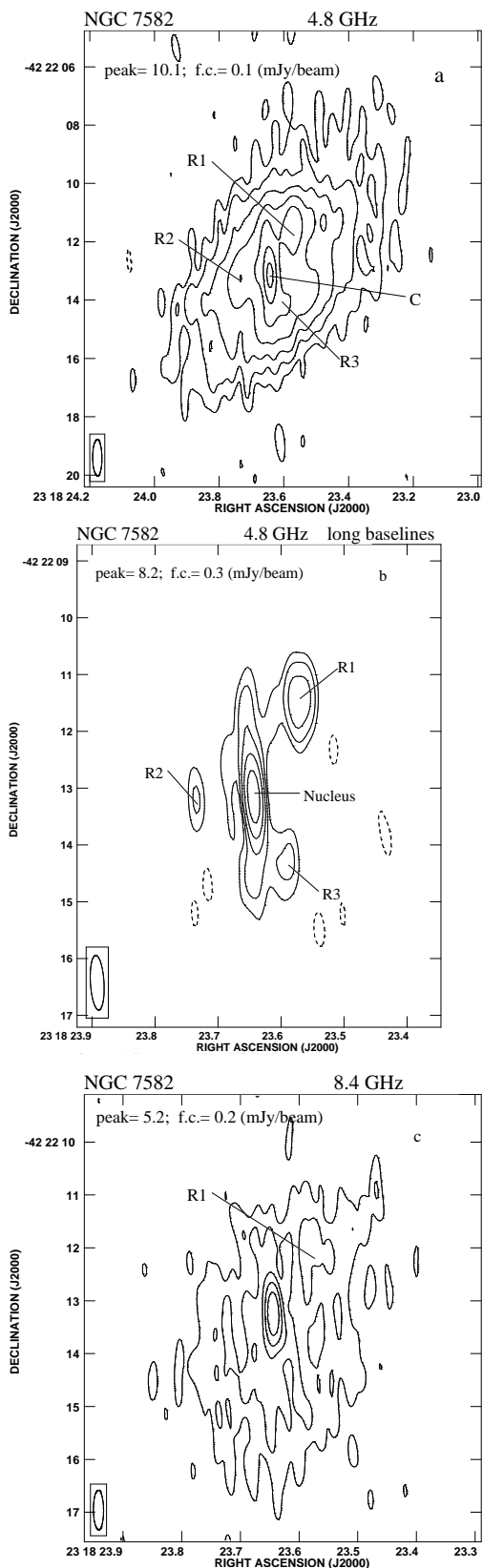


**Figure 7.** VLA images of the central region of NGC 7582 at 4.8 GHz (*top*), without the shortest baselines (*centre*), and at 8.4 GHz (*bottom*). On each image we provide the observing frequency; the restoring beam, plotted on the bottom left corner; the peak flux density in mJy/beam; the first contour intensity (*f.c.* in mJy/beam), that is 3 times the off-source noise level; contour levels increase of a factor 2.

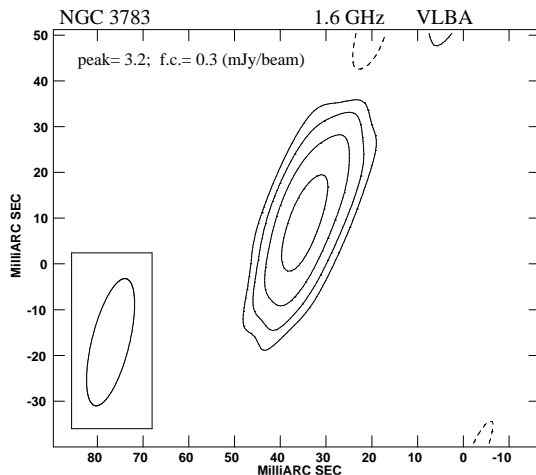


**Figure 8.** VLBA image at 1.6 GHz of the central region of NGC 3783. On the image we provide the observing frequency; the restoring beam, plotted on the bottom left corner; the peak flux density in mJy/beam; the first contour intensity (*f.c.* in mJy/beam), that is 3 times the off-source noise level; contour levels increase of a factor 2.

that is a little flatter than the spectral index of the whole extended emission.

## 5 DISCUSSION

### 5.1 The nuclear radio emission

In general, the nucleus of these Seyfert galaxies is unresolved at the resolution provided by the VLA in its larger configurations (A and B arrays), giving an upper limit to the linear size between about 20 and 120 pc. Only MCG-5-23-16 and NGC 7469 are marginally resolved at the highest resolution (FWHM  $\sim 0.2$  arcsec). In both cases the central component is elongated suggesting a core-jet morphology.

For all the sources we find that the spectral index of the nucleus ranges between 0.5 and 0.9, with the only exception of NGC 1097 where the spectrum is inverted.

When observed with pc-scale resolution, most sources display a resolved structure. This is the case of MRK 1239 (Fig. 4c), NGC 5506 (Middelberg et al. 2004), and NGC 7469 (Lonsdale et al. 2003). MRK 1239 shows a well defined double morphology with a total linear size of 40 pc. The lack of multi-frequency information does not allow us to study the spectral index distribution. NGC 5506 and NGC 7469 are characterised by several compact components resembling a core-jet structure. In NGC 5506, the availability of multi-frequency observations singles out one of the components with a flat spectrum (Middelberg et al. 2004).

NGC 3783 is still unresolved at pc-scale resolution (Fig. 8), and an upper limit to the linear size  $< 4$  pc is estimated.

For the sources with VLBA information, MRK 1239, NGC 3783, NGC 5506, and NGC 7469, an estimate of the brightness temperature  $T_B$ , the equipartition magnetic field  $H_{eq}$  and minimum energy density  $u_{min}$  is provided. We do

not compute physical parameters for the sources unresolved in VLA images because no tight constraints on their values can be derived. To compute the physical parameters of MRK 1239 and NGC 3783 we make use of the values at 1.6 GHz reported in Table 3. In the case of NGC 5506 and NGC 7469 we compute the physical parameters making use of the values reported in Middelberg et al. (2004) and Lonsdale et al. (2003), respectively. The brightness temperature is computed by:

$$T_B = \frac{S(\nu)}{2k \theta_{\text{maj}} \theta_{\text{min}}} \left( \frac{c}{\nu} \right)^2$$

where  $S(\nu)$  is the flux density at the frequency  $\nu$ ,  $\theta_{\text{maj}}$  and  $\theta_{\text{min}}$  are the source major and minor axis,  $k$  is the Boltzmann constant, and  $c$  the speed of light. For the magnetic field and energy density we follow standard formulae (Pacholczyk 1970), assuming equipartition condition between radiating particles and magnetic field. The equipartition magnetic field is

$$H_{\text{eq}} = \sqrt{\frac{2A}{7} \pi u_{\text{min}}}$$

and the minimum energy density  $u_{\text{min}}$  is

$$u_{\text{min}} = 1.04 \cdot 10^{-23} \cdot \left( \frac{L}{V} \right)^{4/7}$$

where  $L$  is the synchrotron luminosity in Watt, and  $V$  the volume of the emitting region in  $\text{pc}^3$ . We assume that the volume of the emitting region is a prolate spheroid

$$V = \frac{\pi}{6} d_{\text{maj}} d_{\text{min}}^2$$

where  $d_{\text{maj}}$  and  $d_{\text{min}}$  are the source linear sizes. We assume a filling factor of unity, i.e. the source volume is fully and homogeneously filled by relativistic plasma. Furthermore, proton and electron energy densities are assumed to be equal. For the Seyfert nuclei with VLBI information, we obtain  $u_{\text{min}}$  of the order of  $10^{-6} - 10^{-7} \text{ erg/cm}^3$ ,  $H_{\text{eq}} \sim 1.5 - 10 \text{ mG}$  and  $T_B$  of about  $10^7 - 10^8 \text{ K}$ . These values are comparable to those derived in the nucleus of other Seyfert galaxies (e.g. Ulvestad & Wilson 1984; Kukula et al. 1999).

## 5.2 The off-nucleus radio emission

Of the seven Seyfert nuclei studied, four (NGC 1097, NGC 5506, NGC 7469 and NGC 7582) are surrounded by diffuse emission extending on kpc scale. In NGC 5506, Wehrle & Morris (1987) suggested that its extended 0.35-kpc halo may be due to either a radio plasma bubble expanding from the AGN, or a magnetically dominated coronal arc. Another possibility is that it is produced by free-free emission from the ionised gas heated by the AGN. However, the steep spectral index  $\alpha = 0.9$  makes the interpretation unlikely, as thermal emission would produce a flatter spectral index. Furthermore, the extended emission does not seem to be related to starburst activity, as no evidence for this is seen in high spatial resolution IR images up to  $20 \mu\text{m}$  (Prieto et al. 2009; Reunanen et al. 2009).

In NGC 1097, NGC 7469 and NGC 7582, the extended emission is resolved in knots (Table 3), each having a counterpart star-forming region in high spatial resolution

IR images (Reunanen et al. 2009). The analysis of the SED of the individual star-forming clumps in these galaxies, from radio to UV, is showing that these regions are young super-massive stellar clusters, analogues to those seen in the starburst nucleus of NGC 253 (Fernandez-Ontiveros et al. 2009). In radio, the spectral index is relatively steep,  $\sim 0.4 - 0.9$  in NGC 1097 (Hummel et al. 1987) and in NGC 7469 (Alberdi et al. 2006), and  $\sim 0.9$  in region R1 of NGC 7582 (no sufficient information is available for the other knots of NGC 7582 to derive the spectral index), suggesting a dominant non-thermal origin, most probably from supernovae events in these clusters. Not all the IR star-forming regions are detected in radio, suggesting different evolution phase of the clusters within the same star-forming ring (Fernandez-Ontiveros et al. 2009, in preparation).

## 5.3 The missing flux density

### 5.3.1 Observational limitations

An interesting characteristic shown by the Seyfert nuclei with VLBI information, namely MRK 1239, NGC 3783, NGC 5506 and NGC 7469, is that their pc-scale flux density is significantly lower than that measured on VLA images even in the presence of unresolved structures. In MRK 1239 and NGC 3783, the flux density derived from VLBA data accounts only for 20% of that measured on VLA images. This suggests that a significant fraction of the radio emission is not concentrated in a compact component at the centre, but it spreads over a region that is slightly larger than  $0''.1$ , i.e. the largest angular scale detectable by the VLBA at 1.6 GHz, and smaller than the resolution of VLA data at the same frequency, that is  $< 0''.3$  for MRK 1239 (see Table 2) and  $< 0''.5$  for NGC 3783 (Ulvestad & Wilson 1984). A strong support to this interpretation comes from observations with different resolution of the nucleus of NGC 7469. In MERLIN observations at 1.6 GHz (Alberdi et al. 2006) the nucleus is slightly resolved on the east-west direction, giving an upper limit to its angular size of about  $0''.15$ . The east-west elongation is confirmed by pc-scale resolution VLBI observations (Lonsdale et al. 2003), where the nucleus is resolved in 5 components spread over an area of about  $0''.17$ , i.e. comparable to that derived from MERLIN data. However, the flux density recovered from VLBI data accounts only for  $\sim 50\%$  of that measured on MERLIN images. A similar result was found in NGC 5506 by Middelberg et al. (2004), where EVN observations of the nucleus could recover only 43% of the flux density measured by MERLIN. In this case, an extended, low-surface brightness region, detected by MERLIN, is not seen by the EVN, as it is insensitive to structures larger than 35 mas at 18 cm, and 11 mas at 6 cm.

From these results we can argue that in the case of NGC 5506 and NGC 7469, the missing flux density on VLBI image is likely due to diffuse, steep-spectrum low-surface brightness emission that is undetectable by VLBI observations either due to sensitivity limitation or because the structure is larger than the maximum scale detectable by the interferometer, or a combination of both. A similar result was found in the case of the Seyfert NGC 1068 where

Gallimore et al. (2004) noted that deep VLBA observations could detect a flux density almost 50% higher than that of lower sensitivity VLBA observations by Roy et al. (1998), but still the total flux density measured on images with lower spatial resolution could not be recovered.

### 5.3.2 Steep-spectrum versus flat-spectrum Seyfert nuclei

The fact that in Seyfert nuclei the pc-scale radio emission does not account for all the flux density measured at lower resolution, even in the presence of an unresolved component, was already noted by Sadler et al. (1995) by studying a sample of 22 nearby Seyferts with the PTI. They suggested that in Seyfert galaxies the radio emission is more diffuse and less centrally concentrated than in elliptical radio galaxies. A similar behaviour was also found by Lal et al. (2004) by comparing simultaneous VLA and VLBI observations of a sample of Seyfert galaxies. They found that in  $\sim 60\%$  of the sources more than half of the VLA flux density of the unresolved component is missing in VLBI images.

However, evidence of undetected flux density on pc-scale is not a characteristic common to all Seyfert nuclei. For example, it has been found that in flat-spectrum Seyfert nuclei essentially all the emission on arcsecond scale is present on VLBI scales (Anderson et al. 2004; Anderson & Ulvestad 2005), indicating that all the radio emission is concentrated in the central component. On the other hand, in Seyfert nuclei characterised by a steep spectrum, the flux density recovered on mas-scales is usually significantly lower than that expected from arcsecond-scale images, suggesting that the radio emission is not centrally concentrated, but it is diffuse on a larger region. A noticeable example of a steep-spectrum Seyfert nucleus where the flux density almost disappears moving from arcsec to milli-arcsec scales is represented by NGC 4151, where only 8% of the flux density from the central component could be recovered by VLBI observations (Pedlar et al. 1993; Ulvestad et al. 1998), while a large fraction of the jet emission is undetected. This suggests that in Seyfert nuclei unresolved on arcsec scale but with different spectral index properties, the dominant radio emission may originate from different features: from the central core in flat-spectrum objects, from extended features, like jets, in steep-spectrum nuclei.

### 5.3.3 Thermal or non-thermal origin?

So far, the nature of the missing flux density has not been investigated in detail. This diffuse emission may be due to either thermal emission from ionised gas heated by the AGN, or by nuclear star forming regions, or non-thermal radiation from the AGN itself.

To investigate a possible free-free origin of the missing flux we compute the electron density  $n_e$  that the ionised gas must have in order to emit the “missing” flux density:

$$n_e^2 = 1.84 \times 10^{41} \left( \frac{T}{10^4 \text{K}} \right)^{1/2} D_L^2 S(\nu) V^{-1} g_{\text{ff}}^{-1} \quad (1)$$

where  $D_L$  is the luminosity distance,  $T$  is the gas temperature in units of  $10^4$  K, and  $g_{\text{ff}}$  the Gaunt factor. In Eq. 1 we assumed that electrons and protons have the same density. At radio frequency,  $g_{\text{ff}} \sim 17.7 + \ln(T^{3/2}/\nu)$  (e.g. Pacholczyk 1970). We assume the gas temperature  $T \sim 10^4 - 10^6$  K. The missing flux is calculated as the difference between the VLA and VLBI flux densities. In the case of MRK 1239 and NGC 3783, the missing flux at 1.6 GHz is  $\sim 50$  and 18 mJy, respectively. If we consider these parameters in Eq. 1, we obtain an upper limit to the electron density  $n_e \sim 10^3 - 10^4 \text{cm}^{-3}$ , over a spherical volume of 0.1 arcsec (i.e. 57 and 20 pc for MRK 1239 and NGC 3783 respectively) in diameter. This value is the largest angular size detectable from the VLBA, (i.e. the VLBA at 1.6 GHz is insensitive to structures larger than  $0''.1$ ) and it represents, therefore, a lower limit to the source size. Such a dense gas would completely absorb the synchrotron emission arising from the embedded AGN:

$$S_{\text{obs}}(\nu) = S_0(\nu) e^{-\mu(\nu)l} \quad (2)$$

where  $S_{\text{obs}}$  and  $S_0(\nu)$  are the observed and the intrinsic flux density at the frequency  $\nu$  respectively,  $l$  is the width of the ionised region, and  $\mu(\nu)$  the absorption coefficient at the frequency  $\nu$  (Rybicki & Lightman 1979). At radio wavelengths

$$\mu(\nu) \sim 0.018 T^{-3/2} n_e^2 \nu^{-2} g_{\text{ff}}.$$

We consider that the pc-scale structure found in the VLBA images (Figs. 4c and 8) arises from the central AGN and the observed flux density is 10 mJy and 5 mJy for MRK 1239 and NGC 3783 respectively. We assume that the AGN is located in the centre of the ionised region, i.e.  $l$  is equal to the radius of the ionised sphere (Fig. 9) that accounts for 28.5 pc and 10 pc in the case of MRK 1239 and NGC 3783, respectively. With this parameters in Eq. 2 we obtain an intrinsic flux density arising from the central AGN that is much higher than a few thousands of Jy. This suggests that the “missing” flux is not free-free from gas ionised by the central AGN, and a non-thermal AGN-related origin is more plausible.

Another possibility may be that the ionised gas is related to an HII region located in projection behind the AGN, or that the gas around the AGN is not ionised uniformly. In this way, our line of sight to the central AGN does not pass through the ionised gas, thus avoiding any absorption of the AGN radiation.

However, a strong support to the non-thermal synchrotron origin of the diffuse emission comes from the comparison, when possible, between the spectral index distribution in low and spatial resolution images. For example, in the case of NGC 5506, the unresolved nucleus in VLA data has a steep spectrum with a mean value  $\alpha \sim 0.8$ , while at pc-scale resolution (Sadler et al. 1995) the spectrum has a convex shape with the peak occurring around 3.5 GHz. This suggests that a significant fraction of steep-spectrum, low-surface brightness emission is present in the nuclear region, but it cannot be detected in VLBI observations likely due to observational limitations.

As in the case of NGC 4151 (Ulvestad et al. 1998), the steep emission may arise from a jet, that may be distorted and/or disrupted by the dense ambient medium. For example on arcsecond scale, NGC 4151 displays a compact core and two collimated jets (Pedlar et al. 1993; Kukula et al. 1995).

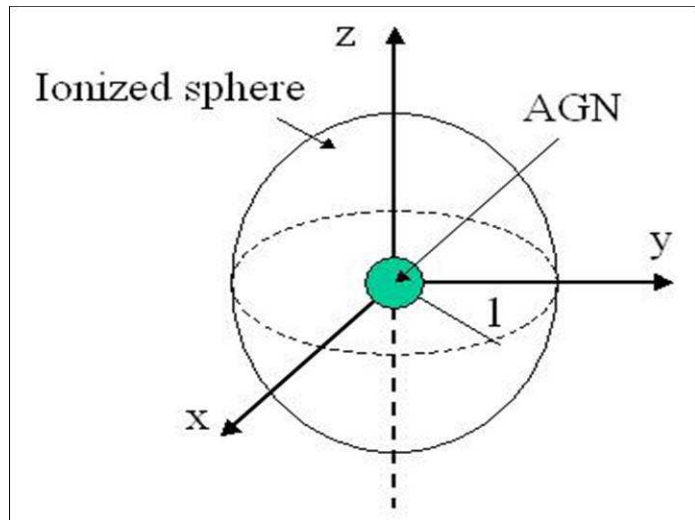


**Figure 9.** The assumed geometry for the ionised gas heated by the AGN. The AGN is located in the centre of the ionised sphere with an angular diameter of 0.1 arcsec, that corresponds to the largest region detectable by the VLBA at 1.6 GHz.

When observed with higher resolution, the compact core is resolved in several knots forming a jet which is not aligned with the arcsec-scale jet (Ulvestad et al. 1998). The misalignment often found between the radio jets on milli-arcsecond scale and those on larger scale (Ulvestad et al. 1998) may be an evidence of the interaction between the radio jet and the environment. In this scenario it is also possible that, for some reason, flat-spectrum Seyfert nuclei are not able to develop a radio jet, and this causing that all their emission is produced in the central compact component.

## 6 CONCLUSIONS

We presented the analysis of multi-frequency archival VLA and VLBA data of 7 close and bright Seyfert nuclei. The conclusions we can draw from this investigation are:

- At VLA resolution, FWHM  $\sim 0''.1$ , the nucleus of the Seyfert galaxies is unresolved, with the only exception of MGC-5-23-16 and NGC 7469 which show a core-jet structure. At VLBA resolution, equivalent to a few parsecs, the nucleus of MRK 1239 is resolved in two components, while in NGC 3783 it is still unresolved.

- The Seyfert galaxies in this study with known circumnuclear star-forming regions in the IR, namely NGC 1097, NGC 7469 and NGC 7582 (Reunanen et al. 2009) present a radio counterpart for a few ( $\sim 10\%$ ) of these regions. Most are not detected in radio, indicating that those detected may be characterised by higher supernovae rate. Their steep radio spectral index is in line with this idea. Conversely, none of the other Seyfert nuclei present any circumnuclear

radio emission. The only exception is NGC 5506 that shows a radio halo surrounding the nucleus.

- A comparison between arcsecond and milli-arcsecond resolution in MRK 1239 and NGC 3783, pointed out that almost 80% of the radio flux density detected in VLA observations is not recovered at pc-scale resolution. This suggests the presence of a diffuse component on scales of a few tens of parsecs, undetected with the VLBA. Similar situation is found in NGC 1068, NGC 4151, NGC 5506 and NGC 7469. The nature of this “missing” flux components is likely due to synchrotron AGN-related emission. This difference between the flux density measured on arcsecond and milli-arcsecond resolution images is not found in the case of elliptical radio galaxies, but it appears to be a common phenomenon in Seyfert galaxies with a steep spectrum, mostly hosted in spirals. If of synchrotron origin, this emission may be spilt off from a jet that may get easily distorted and/or disrupted by the dense interstellar medium in the nucleus of spirals.

- A comparison between Seyfert nuclei with different spectral properties points out that in flat-spectrum nuclei, almost all the flux density is recovered on milli-arcsecond scale. This indicates that in flat-spectrum objects the radio emission is essentially concentrated in the compact core, without evidence of jet-like structure even on milli-arcsecond scale, while in steep-spectrum objects a significant fraction of the radio emission arises from low-surface brightness, extended features.

## ACKNOWLEDGEMENTS

We thank the anonymous referee for carefully reading the manuscript and valuable suggestions. The National Radio Astronomy Observatory is a facility of the National Science Foundation operated under cooperative agreement by Associated Universities, Inc. This work has made use of the NASA/IPAC Extragalactic Database NED which is operated by the JPL, Californian Institute of Technology, under contract with the National Aeronautics and Space Administration.

## REFERENCES

- Alberdi, A., Colina, L., Torrelles, J.M., Panagia, N., Wilson, A.S., Garrington, S.T., 2006, *ApJ*, 638, 938
- Anderson, J.M., Ulvestad, J.S., Ho, L.C., 2004, *ApJ*, 603, 42
- Anderson, J.M., Ulvestad, J.S., 2005, *ApJ*, 627, 674
- Fernandez-Ontiveros, J.A., Prieto, M.A., Acosta-Pulido, J.A., *MNRAS*, 392L, 16
- Gallimore, J.F., Baum, S.A., O’Dea, C.P., 2004, *ApJ*, 613, 794
- Hagiwara, Y., Diamond, P.J., Nakai, N., Kawabe, R., 2000, *A&A*, 360, 49
- Hummel, H., van der Hulst, J.M., Keel, W.C., 1987, *A&A*, 172, 32
- Kukula, M.J., Pedlar, A., Baum, S.A., O’Dea, C.P., 1995, *MNRAS*, 276, 1262

- Kukula, M.J., Ghosh, T., Pedlar, A., Schilizzi, R.T., 1999, ApJ, 518, 117
- Lal, D.V., Shastri, P., Gabuzda, D.C., 2004, A&A, 425, 99
- Lonsdale, C.J., Lonsdale, C.J., Smith, H.E., Diamond, P.J., 2003, ApJ, 592, 804
- Middelberg, E., Roy, A.L., Nagar, N.M., et al., 2004, A&A, 417, 925
- Momjian, E., Romney, J.D., Carilli, C.L., Troland, T.H., 2003, ApJ, 597, 809
- Morganti, R., Tsvetanov, Z.I., Gallimore, J., Allen, M.G., 1999, A&AS, 137, 457
- Nagar, N.M., Wilson, A.S., Falcke, H., 2001, ApJ, 559, 87
- Pacholczyk, A.G., 1970, Radio Astrophysics (San Francisco: Freeman & Co.)
- Pedlar, A., Kukula, M.J., Longley, D.P.T., et al., 1993, MNRAS, 263, 471
- Prieto, M.A., et al., 2009, MNRAS submitted
- Reunanen, J., Prieto, M.A., Siebenmorgen, R., 2009, MNRAS submitted
- Roy, A.L., Colbert, E.J.M., Wilson, A.S., Ulvestad, J.S., 1998, ApJ, 504, 147
- Rush, B., Malkan, M.A., Edelson, R.A., 1996, ApJ, 473, 130
- Rybicki, G.B., Lightman, A.P., 1979, Radiative Processes in Astrophysics, (New York: John Wiley & Son)
- Sadler, E.M., Slee, O.B., Reynolds, J.E., Roy, A.L., 1995, MNRAS, 276, 1373
- Schmitt, H.R., Ulvestad, J.S., Antonucci, R.R.J., Kinney, A.L., 2001, ApJS, 132, 199
- Storchi-Bergmann, T., Baldwin, J.A., Wilson, A.S., 1993, ApJ, 410, 11
- Thean, A., Pedlar, A., Kukula, M.J., Baum, S.A., O'Dea, C.P., 2000, MNRAS, 314, 573
- Thean, A.H.C., Gillibrand, T.I., Pedlar, A., Kukula, M.J., 2001, MNRAS, 327, 369
- Trotter, A.S., Greenhill, L.J., Moran, J.M., et al., 1998, ApJ, 495, 740
- Ulvestad, J.S., Wilson, A.S., Sramek, R.A., 1981, ApJ, 247, 419
- Ulvestad, J.S., Wilson, A.S., 1984, ApJ, 285, 439
- Ulvestad, J., Neff, S., Wilson, A., 1987, AJ, 93, 22
- Ulvestad, J.S., Antonucci, R.R.J., Goodrich, R.W., 1995, AJ, 109, 81
- Ulvestad, J.S., Roy, A.L., Colbert, E.J.M., Wilson, A.S., 1998, ApJ, 496, 196
- Unger, S.W., Pedlar, A., Booler, R.V., Harrison, B.A., 1986, MNRAS, 219, 387
- Wehrle, A.E., Morris, M., 1987, ApJ, 313, 43
- Wilson, A.S., Helfer, T.T., Haniff, C.A., Ward, M.J., 1991, ApJ, 381, 79
- Wrobel, J.M., 1984, ApJ, 284, 531